Desalination and Water Treatment
www.deswater.com

doi: 10.5004/dwt.2017.20628

74 (2017) 316–325
May

Optimized routes for the preparation of gadolinium carbonate and oxide nano-particles and exploring their photocatalytic activity

Seied Mahdi Pourmortazavi[a,*], Mehdi Rahimi-Nasrabadi[b,c,*], Mustafa Aghazadeh[d], Mohammad Reza Ganjali[e,f], Meisam Sadeghpour Karimi[e], Parviz Norouzi[e,f]

[a]*Faculty of Material and Manufacturing Technologies, Malek Ashtar University of Technology, P.O. Box 16765-3454, Tehran, Iran, Fax: +98-212-2936578; email: pourmortazavi@yahoo.com*
[b]*Faculty of Pharmacy, Baqiyatallah University of Medical Sciences, Tehran, Iran, email: rahiminasrabadi@gmail.com*
[c]*Department of Chemistry, Imam Hossein University, Tehran, Iran*
[d]*Nuclear Science and Technology Research Institute (NSTRI), P.O. Box 14395–834, Tehran, Iran, email: Mustafa.aghazadeh@gmail.com*
[e]*Center of Excellence in Electrochemistry, University of Tehran, Tehran, Iran, emails: ganjali@khayam.ut.ac.ir (M.R. Ganjali), mesa1363@yahoo.com (M.S. Karimi), norouzi@khayam.ut.ac.ir (P. Norouzi)*
[f]*Biosensor Research Center, Endocrinology & Metabolism Molecular-Cellular Sciences Institute, Tehran University of Medical Sciences, Tehran, Iran*

Received 08 September 2016; Accepted 26 February 2017

ABSTRACT

A sequence of organized precipitation test was conducted based on the Taguchi robust design so as to evaluate the best conditions for the preparation of $Gd_2(CO_3)_3$ nano-particles in the absence of common additives like surfactants, templates or catalysts, indicating that the dimensions of the product nano-particles can be manipulated merely through altering the parameters affecting the reaction. These parameters include the concentrations of Gd(III) and carbonate ions as well as the reactor temperature. The optimal reaction conditions led to the production of $Gd_2(CO_3)_3$ nano-particles of 36 nm in average diameter, which were evaluated by scanning electron microscopy (SEM), fourier transform infrared spectroscopy (FT-IR), thermogravimetric-differential thermal analysis, and UV–Vis spectrophotometry. $Gd_2(CO_3)_3$ was further calcinated at 700°C to decompose into spherical Gd_2O_3 nano-particles with average diameters below 25 nm, the formation of which was established by SEM, X-ray diffraction (XRD), and FT-IR techniques. In order to obtain the band gap energies of the fabricated carbonate and oxide nano-products, they were characterized by UV–Vis diffuse reflectance spectroscopy (DRS). Besides, the photocatalytic behaviors of the nano-products in degradation of methyl orange as a pollution of water were explored, and the results exhibited the efficacy of both products in eliminating of the organic pollutant.

Keywords: Nano-structures; Lanthanides oxide; Chemical synthesis; Photocatalyst; Gadolinium carbonate

1. Introduction

Due to the exceptional optical and magnetic properties, nano-structures of lanthanides have turned out as likely candidates for application as luminescent biomarkers or contrast agents in magnetic resonance imaging. More specifically, the use of oxide of gadolinium, in high-k gate dielectrics, has been of incremental interest in complementary metal-oxide-semiconductor (CMOS) technologies [1]. Gd_2O_3 has further been used as a promising candidate for application in III-V CMOS, due to it can be allowed to have a charge matching with the Ga–As interface [2]. Gadolinium oxide also has applications in dimerization catalysts [3], neutron converters in imaging plate neutron detectors [4], as additives in UO_2 fuel rods for nuclear reactors [5]; for enhancing the toughness of ZrO_2 [6]; for boosting densification of SiC

* Corresponding author.

and Si_3N_4 [7,8]; and for enhancing the sintering properties of CeO_2 in fuel cells [9]. The use of Eu-doped gadolinium oxide in ultraviolet detectors [10] and scintillators coupled with a CCD-TV camera for high-resolution X-ray medical imaging [11] has also been described. The possibility of application of ultrafine Gd_2O_3 powder is rather desirable in many of these applications.

Many synthesis routes have been proposed for the preparation of oxides of rare earths [12,13], but little has been published on the specifics of the synthesis of Gd_2O_3. The compound is conventionally prepared by the thermal decomposition of precursor compounds like $Gd(CH_3COO)_3{\cdot}4H_2O$ [3], $Gd(OH)CO_3$ [14], and $Gd(OH)_3$ [15,16]. Obviously various routes have their benefits and drawbacks, and hence selection of a suitable procedure for the preparation of the product necessitates the consideration of numerous features including the complication, time, cost affectivity, etc. Consequently, alternative synthesis routes for synthesizing rare earth oxide especially in nano-scales are always desirable.

Nano-technology as the knowledge of the materials at the molecular scales (considerably lower than 100 nano-meters) permits preparation of the materials with manipulated properties. Among the widespread application of the nano-structured materials, heterogeneous photocatalysis gained considerable attention recently [17,18] due to the importance of this area in addition to the malleable character of the resulted solutions from it. Photocatalysis generally is dealing with the extending of the light to a variety of processes, i.e., oxidative cleavages, oxidations, isomerizations, reductions, polymerizations, and substitutions condensations. Prolonging the concept of nano-technology to the heterogeneous catalysis could be useful for the more accurate understanding of the occurred transformations on the surface of catalyst at the molecular levels [19,20]. Furthermore, fabrication of the materials with nano-sized dimensions could facilitate understanding of their reaction mechanisms and hence designing novel catalytic systems [21–23].

The organic pollutants presented in wastewater may cause serious environmental difficulties. Organic dyes as water pollutants are chemically stable, and their decomposition and degradation to the safe ingredients are important threat to the surrounding environments. Elimination of color from wastewater today is a challenging necessities countered in textile, dye, and paper industries [24,25]. On the other hand, lanthanides are renowned for their proficiency in formation of complexes with Lewis bases (i.e., thiols, aldehydes, amines, etc.) via interacting the base functional groups with the *f*-orbitals of the lanthanides. Consequently, lanthanide derivatives compounds might deliver gorgeous photocatalytic activities and are proposed for employing in polluted water treatment.

Precipitation is among the first chemical techniques used for the preparation of insoluble salts, i.e., gadolinium carbonate [26,27]. Although rather simple, the method requires the precise control of the characteristics of the product with respect to its size, shape, chemical composition, and substructure. As results, a great deal of work has been directed toward gaining control over such reactions, which produce single crystals or poly-crystals composed of a large number of small crystals. The formation of single crystals can be explained by the classic nucleation and growth theory [28–31]. The inherently unstable nano-particles, which readily aggregate to form larger particles, are often the main product of the precipitation routes [28–33].

The dimensions of precipitation products are greatly influenced by experimental conditions that can be optimized by means of an orthogonal array design (OAD) [33–35], which is a style of fractional factorial design where an orthogonal array is used for assigning the chief factors for a set of experimental combinations [36]. The method helps characterize a complicated process in fewer numbers of experiments; however, the proper setup of the test mandates a specialized design experiment, further to the specialized statistics needed for the interpretation of the results [35–38]. During multilevel OADs, one parameter is considered at more than two levels, and hence a significant curvature in the response surface can satisfy the nonlinear character [39,40]. The OAD results are next analyzed through analysis of variance (ANOVA) to gain object information explaining and confirming the significance of the experimental factors studied [41–43].

What we focused on was optimizing the factors influencing the direct precipitation reaction (DPR) leading to the formation of $Gd_2(CO_3)_3$ nano-particles, through a statistical experiment design. Next the composition and morphology of the product particles were investigated, and the product was thermally treated so as to produce Gd_2O_3 by thermal decomposition, and the optimum conditions of this latter reaction were also evaluated by thermal analyses. Moreover, degradation of methyl orange (MO) was followed as a test reaction to explore photocatalytic behaviors of the fabricated gadolinium carbonate and gadolinium oxide nano-particles.

Several reports on the synthesis of gadolinium carbonate and oxide micro- and nano-particles through a variety of techniques have been published [3,14–17], but none has focused on the synthesis of the two compounds via controlled precipitation and thermal decomposition of the precipitation product in the absence of surfactants, templates, and/or catalysts.

2. Experimental setup

2.1. Optimization of the precipitation reaction

Gadolinium chloride and sodium carbonate salts of analytical grade were purchased from Merck (Darmstadt, Germany) and used without any treatment. $Gd_2(CO_3)_3$ particles were synthesized by adding different Gd^{3+} solutions of several concentrations to carbonate solutions at different flows, vigorous stirring and different reactor temperatures. After the formation of the particles, they were filtered and washed with distilled water 3 times and next with ethanol and dried at 70°C for 4 h.

The variables used for the experimental design were the concentrations of Gd^{3+} and CO_3^{2-} solutions as well as the flow rate at which Gd^{3+} was added to CO_3^{2-}, and the reactor temperature, which were studied at three different levels as shown in Table 1.

2.2. Decomposition of $Gd_2(CO_3)_3$

Gd_2O_3 nano-particles were prepared through the thermal decomposition of $Gd_2(CO_3)_3$, which was synthesized in the initial DPR under the optimum conditions. The decomposition reaction was performed in furnace under static air atmosphere at 700°C for 4 h. During the tests, 0.3 g samples of $Gd_2(CO_3)_3$ was loaded into a 40-mm width and 20-mm height

Table 1
Orthogonal array used for parameter optimization during gadolinium carbonate synthesis by direct precipitation reaction while mean diameter of gadolinium carbonate are as response

Experiment number	Gd^{3+} concentration (M)	CO_3^{2-} concentration (M)	Gd^{3+} feed flow rate (mL/min)	Temperature (°C)	Diameter of gadolinium carbonate particles (nm)
1	0.01	0.01	2.5	0	44
2	0.01	0.05	10.0	30	36
3	0.01	0.25	40.0	60	46
4	0.05	0.01	10.0	60	43
5	0.05	0.05	40.0	0	46
6	0.05	0.25	2.5	30	48
7	0.25	0.01	40.0	30	52
8	0.25	0.05	2.5	60	51
9	0.25	0.25	10.0	0	68

crucible made of alumina, which was covered with copper foil after sample loading, to avoid the loss of the powder during the decomposition process. The product was finally collected and used for further analysis.

2.3. Characterization of nano-scale products

Morphology of samples of all products was studied by scanning electron microscopy (SEM) tests using a Philips XL30 series instrument. The samples were loaded into the instrument using gold films prepared using a sputter coater model SCD005 produced by BAL-TEC (Switzerland).

A Ziess EM900 scanning electron microscope was used to acquire the transmission electron microscope (TEM) images. The samples used for TEM were coated on Cu-carbon coated grids. X-ray diffraction (XRD) tests were carried out with a Rigaku D/max 2500V diffractometer equipped with a graphite monochromator and a Cu target. A Brucker Equinox 55FT-IR spectrophotometer and KBr pellet technique were used for acquiring the infrared (IR) spectra.

The solid samples were subjected to UV–Vis diffuse reflectance spectra (UV–Vis DRS) studies, and the organic contents of the photocatalytically treated water samples were studied by UV–Vis spectrophotometry. The UV–Vis DRS studies were performed on an Avantes spectrometer (Avaspec-2048-TEC), and the quantitative analyses were performed using a PerkinElmer Lambda 25 UV/Vis spectrometer.

The thermogravimetric-differential thermal analysis (TG-DTA) results were acquired using a thermobalance Stanton, model TR-01 coupled with a differential thermal analysis attachment (STA 1500). During these tests 5.0 mg of $Gd_2(CO_3)_3$ and a reference (Pt foil) were placed in alumina pans and heated at a rate of 10°C/min from 40°C to 800°C, while nitrogen gas was blown at 50 mL/min at 1 bar.

2.4. Diffuse reflectance spectroscopy (DRS)

The purpose of the UV–Vis DRS studies was to evaluate the optical band gap energy (OBGE) values for the synthesized nano-particles. OBGE is defined as the minimum optical energy required for transferring an electron from the valence band of a semiconductor to its conduction band. The relationship between the absorption edge of a semiconductor and energy is as follows [44]:

$$\alpha h\upsilon = A(h\upsilon - E_g)^{\eta} \quad (1)$$

where h, υ, α, E_g, and A, respectively, are the Planck's constant, frequency of light, absorption coefficient, band gap energy, and a constant, while η is ½ since the transition mechanism is direct for the gadolinium salts under study.

2.5. Evaluation of the photocatalytic activity

The gadolinium carbonate and oxide nano-particles were evaluated as photocatalysts in the UV-induced degradation of MO in water samples. The reaction was performed in cylindrical Pyrex double pipe air-lift photoreactor, and the UV irradiation was from a (250 W, $\lambda > 254$ nm) high pressure Hg lamp positioned inside the reactor.

The reaction mixture was a suspension of 0.05 g of the synthesized nano-materials in 0.5 L of a 5 mg/L MO solution and was prepared by magnetically stirring it in the dark for 20 min. Before the onset of the reaction and at 10 min intervals from it samples were taken from the reaction suspension and analyzed to evaluate their MO content by UV–Vis spectrometry at the λ_{max} of MO. The reaction mixture was kept at 25°C through the course of the reaction. The UV–Vis absorbance (A) values were used to calculate the MO concentration (C) of the sample solutions by the Beer–Lambert equation (Eq. (2)) [45]:

$$A = \varepsilon bC \quad (2)$$

in which ε represents the molar absorptivity, and b is the length of the path length occupied by the sample. Considering A_0 and A_t as the absorbance of the samples taken before the reaction and at time t, respectively, and C_0 and C_t as the corresponding concentrations, we have Eqs. (3) and (4):

$$\frac{A}{A_0} = \frac{C}{C_0} \quad (3)$$

$$\text{Degradation efficiency of the catalyst (\%)} = \frac{A_0 - A_t}{A_0} \times 100 \quad (4)$$

The photocatalytic kinetics of the nano-structures was evaluated as opposed to Langmuir–Hinshelwood kinetics model, which is expressed as follows [2–3]:

$$-\frac{dC}{dt} = k_{app}C \quad (5)$$

and is used in the case of photocatalytic degradation of organic molecules at low initial concentration (C = concentration of the organic species, k_{app} = rate constant of the reaction, t = degradation reaction time, $-\frac{dC}{dt}$ = reaction rate).

3. Results and discussion

Given the applicability of DPR for the synthesis of insoluble materials [45,46], and the importance of controlling the size and morphology of the product through optimizing the different influencing parameters, a Taguchi robust design was applied so as to define the interrelations of the various parameters, i.e., Gd^{3+} and CO_3^{2-} concentrations, Gd^{3+} addition flow rate and the reaction temperature, and the results are given in Table 1.

The SEM images of the $Gd_2(CO_3)_3$ samples obtained through DPR at various conditions of Table 1 are given in Fig. 1. It was observed that all samples prepared under the different conditions had spherical morphologies and their diameters varied depending on the conditions as illustrated in Table 1.

To determine the effect of changing the levels of various factors on the dimensions of the product, the average effect of each factor at any level was calculated [37–43]. According to Fig. 2, the mean values for three levels of a factor reveal the product size behavior upon changing the level of the factor. Fig. 2(a) shows that altering the Gd^{3+} and CO_3^{2-} concentrations at three different levels (0.01, 0.05, and 0.25 mol/L) greatly influences the product dimensions. Further, the ANOVA results summarized in Table 2 indicate that both of these concentrations are critical in the determination of particle size.

The effect of varying the Gd^{3+} addition flow rate (i.e., 2.5, 10, and 40 mL/min) on the particle size is shown in Fig. 2(b). The ANOVA results in Table 2 further indicated the flow rate as an insignificant parameter in determining the size of the product while based on Fig. 2(b), an opposite conclusion can be made about the reactor temperature, which is further confirmed by the results of ANOVA in Table 2. Based on the ANOVA results in Table 2, with 90% of confidence

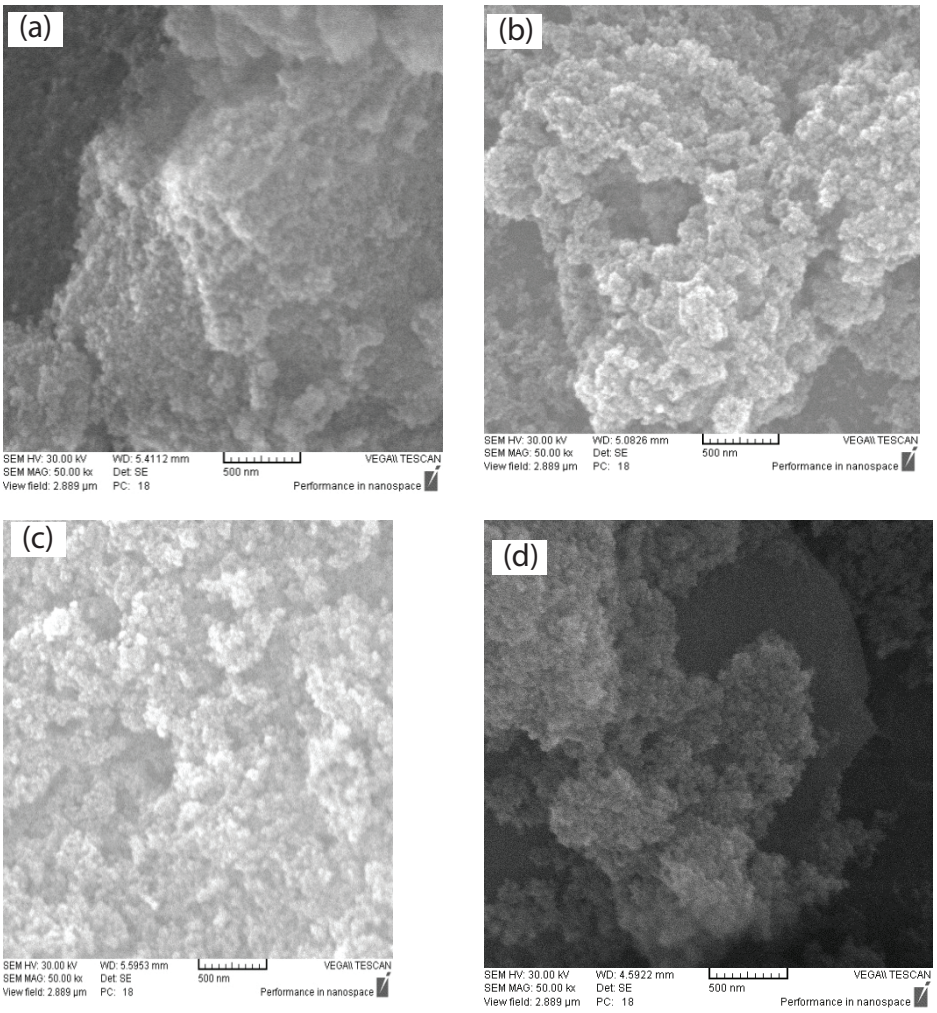

Fig. 1. SEM images of gadolinium carbonate nano-particles obtained under different runs of precipitation reaction (shown in Table 1): (a) run 2, (b) run 4, (c) run 6, and (d) run 8.

all parameters except for the flow rate of adding Gd^{3+} to the reactor play significant roles in determining the diameter of $Gd_2(CO_3)_3$ nano-particles. It should be noted that the interactions among the different variables have been ignored in this work. Based on the ANOVA results and the effects of altering the levels in Fig. 2, it was concluded that the minimum product dimension can be achieved with 0.01 and 0.05 M as the Gd^{3+} and CO_3^{2-} concentrations respectively, and 30°C as the reactor temperature.

The maximum performance of the procedure based on Taguchi experiment design [32–34] is given as follows:

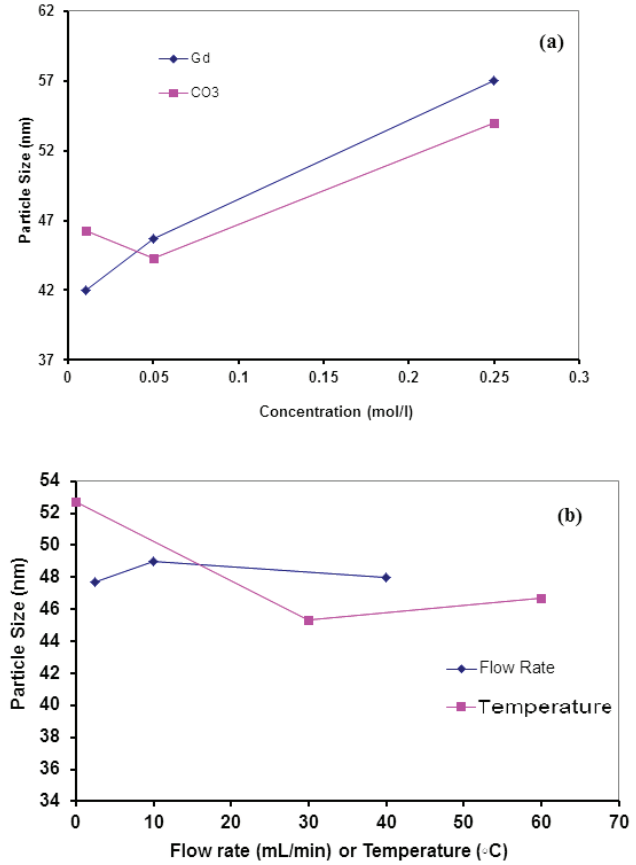

Fig. 2. Average effects of different levels for each variable of precipitation reaction on the diameter of the gadolinium carbonate particles.

$$Y_{opt} = \frac{T}{N} + \left(C_x - \frac{T}{N}\right) + \left(C_y - \frac{T}{N}\right) + \left(T_z - \frac{T}{N}\right) \quad (6)$$

where T/N is the average diameter of the produced particles (T being the grand total of all results and N being the total number of results obtained by experiments in Table 1); Y_{opt} is the diameter of product prepared under the optimal conditions; and C_x, C_y, and T_z represent the optimum Gd^{3+}, CO_3^{2-} and reactor temperature, respectively. Under the optimal conditions, the confidence interval (CI) for the particle size is calculated using [40–42]:

$$CI = \pm\sqrt{\frac{F_\alpha(f_1, f_2)V_e}{N_e}} \quad (7)$$

where $F_\alpha(f_1,f_2)$ concerns with the F value at the degrees of freedom (DOF) f_1 and f_2 at the significance level of 90%, which is achieved from statistical F tables: f_1 = DOF of the mean (always is one), f_2 = DOF for the pooled error term, N_e = effective replications number, while is given by N_e = trials number/(DOF of mean (always is one) + total DOF of factors utilized for the prediction). Calculations for the particle size of the product was prepared under optimal conditions, and CI for the calculated particle size indicated that at a 90% confidence level, the size of the product particles is 35 ± 3 nm.

The second run in Table 1 covers the optimum conditions for the synthesis based on the ANOVA results (i.e., 0.01 and 0.05 M of Gd^{3+} and CO_3^{2-} and 30°C as the reactor temperature). The SEM results showed that the product particles achieved under the conditions of run 2 are about 36 nm in average diameter (Fig. 1(a)), which is consistent with the estimations. The optimal nano-particles were also studied by TEM (Fig. 3), which confirmed the size (36 nm) and spherical morphology observed by the previous tests. Given these confirmations, the product prepared under the conditions of run 2 was used for further characterization by fourier transform infrared spectroscopy (FT-IR), UV–Vis, and thermal analysis.

3.1. FT-IR, UV–Vis, and thermal analysis of the optimal product

The absorption peak at 3,447 cm^{-1} in the IR spectra of the dried product prepared under the conditions of run 2, which is illustrated in Fig. 4, corresponds to the stretching vibration of the O–H bond and the bending vibration of the

Table 2
Results of ANOVA for optimization of synthesis of gadolinium carbonate nano-particles via precipitation procedure using $OA_9(3^4)$ matrix, while diameter of synthesized gadolinium carbonate particles (nm) are as response

Factor	Code	DOF	S	V	Pooled[a]			
					DOF	S′	F′	P′
Gd^{3+} concentration (mol/L)	C_{Gd}	2	366.9	183.4	2	366.9	127.0	58.9
CO_3^{2-} concentration (mol/L)	C_{Car}	2	156.2	78.1	2	156.2	54.1	24.8
Flow rate (mL/min)	F	2	2.9	1.4	–	–	–	–
Temperature (°C)	T_{em}	2	91.6	45.8	2	91.6	31.7	14.4
Error	E	–	–	–	2	2.9	–	1.9

[a]The critical value was at 90% confidence level; pooled error results from pooling insignificant parameter.

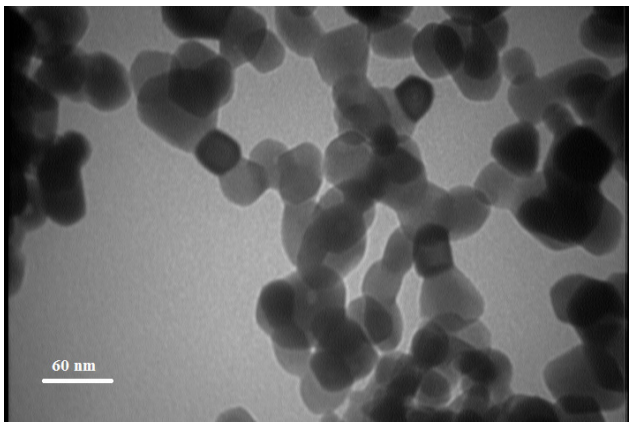

Fig. 3. TEM image of gadolinium carbonate nano-particles obtained via precipitation method under optimum conditions.

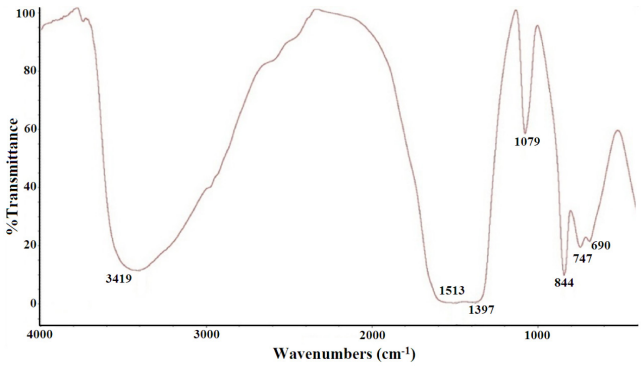

Fig. 4. FT-IR spectrum of gadolinium carbonate nano-particles prepared with precipitation method.

surface absorbed H–O–H [45], while the bands at 1,513 and 1,397 cm^{-1} represent the υ_3 mode of CO_3^{2-} group. The splitting of this band roots in the unequivalence of the crystallographic environment of the CO_3^{2-} ions. Further absorption bands at 1,079, 844, 747, and 699 cm^{-1} also correspond to the stretching states of CO_3^{2-} [37,38].

UV–Vis spectrophotometry was applied to study the optimal product. As it can be seen in Fig. 5, which is the UV–Vis absorption spectrum of the gadolinium carbonate nano-particles dispersed in distilled water, the main absorption by the sample occurs between 240 and 290 nm, which is due to the small crystal size, attributed to the strong quantum confinement of the excitonic transition for nano-structures [46].

DTA and TG techniques, which are used to study the thermal stability of compounds, were also used. Thermal analysis techniques are commonly used prior to the formulation and development of new materials, and here they were applied to determine the thermal stability of the product. Fig. 6 shows the TG-DTA curves of the optimal product. From the TG curve, it is clear that the sample loses ~5% of its mass due to dehydration in the temperature range of 50°C–150°C, before undergoing a continuous decomposition stage in the range of 200°C–600°C [47]. During the decomposition stage, the sample loses about 27% of its mass, but above the temperature of 600°C the sample mass stays almost constant indicating the completion of a decomposition reaction.

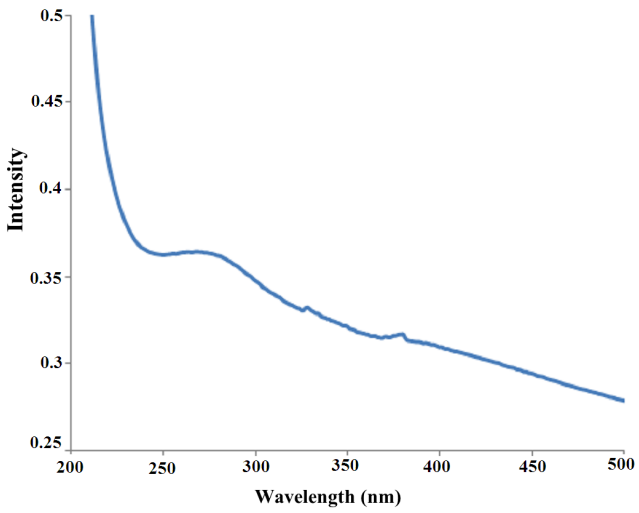

Fig. 5. UV–Vis absorption spectra of the gadolinium carbonate nano-particles (prepared under optimum conditions of precipitation reaction) dispersed in distilled water.

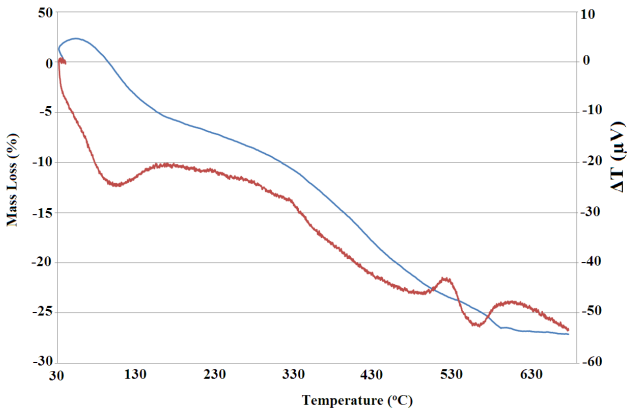

Fig. 6. TG and DTA curves for gadolinium carbonate nano-particles prepared with precipitation method under optimum conditions (sample weight 6.1 mg; heating rate 10°C/min; nitrogen atmosphere).

The complementary DTA data (Fig. 6) showed an endothermic peak at about 110°C that were ascribed to the endothermic nature of the evaporation of water from the surface of the nano-particles. The two endothermic peaks at the higher temperature are indicative of the slow but ongoing decomposing of $Gd_2(CO_3)_3$ into Gd_2O_3 over a wide temperature range. The decomposition is however not one-step, and multiple gadolinium oxides may form intermediate products during the solid-state phase transition. The trend in mass loss of optimum $Gd_2(CO_3)_3$ nano-particles revealed that the decomposition of the precursor completed at the temperature about 600°C, and proper temperatures for obtaining pure Gd_2O_3 by calcination are higher than 600°C.

3.2. *Preparation of Gd_2O_3 by calcination of $Gd_2(CO_3)_3$*

Based on the thermal analysis results described above, Gd_2O_3 nano-particles were prepared by calcinating $Gd_2(CO_3)_3$

nano-particles at 700°C for 4 h in air atmosphere. Fig. 7 illustrates the SEM and TEM images of the acquired Gd_2O_3 particles prepared via this way. The particles possess a spherical structure with an average size of about 23 nm.

The produced nano-particles were further analyzed by XRD and FT-IR spectroscopy techniques. Fig. 8 presents the XRD results for the synthesized Gd_2O_3 nano-particles. It can be seen that all diffraction peaks in the spectrum indicate a cubic phase for the Gd_2O_3 nano-particles, which is in agreement with JCPDS 00–043–1014. This XRD pattern further indicated the crystallinity and purity of the produced powder.

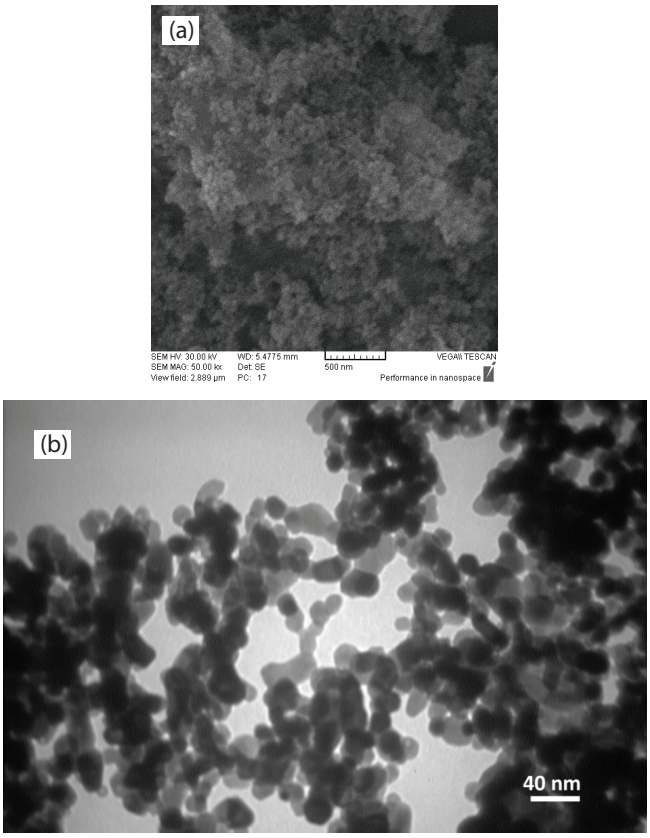

Fig. 7. SEM and TEM images of gadolinium oxide nano-particles obtained via thermal decomposition of precursor.

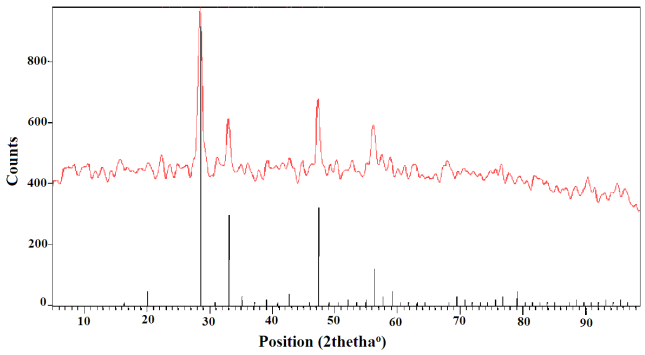

Fig. 8. XRD pattern of the gadolinium oxide nano-particles prepared by thermal decomposition of precursor.

Fig. 9 shows FT-IR spectra of Gd_2O_3 prepared through the calcination of the $Gd_2(CO_3)_3$ precipitate at temperatures of 500°C and 700°C. The FT-IR spectrum of the product of calcination at 500°C shows a reduction in the carbonate absorption band and the emergence of two absorption bands (in comparison with the FT-IR spectrum of the untreated $Gd_2(CO_3)_3$), indicating the formation of cubic phase Gd_2O_3, at 550 and 449 cm^{-1} (Fig. 9(a)). Further calcination of samples at 700°C leads to the complete elimination of carbonate ions and their corresponding bands as well as maturity of the absorption bands of Gd_2O_3 at 552, 455, and 360 cm^{-1} in the FT-IR spectra (Fig. 9(b)). The spectrum of the samples calcinated at 700°C actually contains no additional peaks except for those related to Gd_2O_3 at 552, 455, and 360 cm^{-1} [48].

3.3. UV–Vis diffuse reflectance spectroscopy results

UV–Vis DRS results and Tauc's plots are illustrated in Figs. 10(a) and (b), and Figs. 11(a) and (b), respectively. The experiments showed band gaps to be around 3.75 and 4 eV for the carbonate and oxide sample, respectively. These values are equivalent to respective absorption edges of around 330 and 310 nm.

3.4. Photodegradation activity studies

To assess the photocatalytic activity of the synthesized gadolinium carbonate and oxide nano-particles, MO-containing water solutions were mixed with optimally synthesized nano-structures under the concentration and reaction conditions described above, and samples were taken

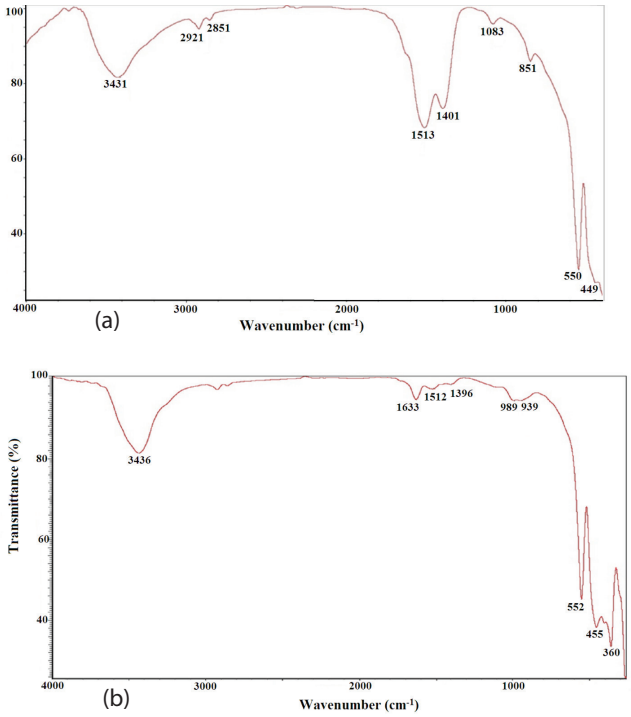

Fig. 9. FT-IR spectrum of gadolinium oxide nano-particles after calcination of precursor at 700°C during 4 h.

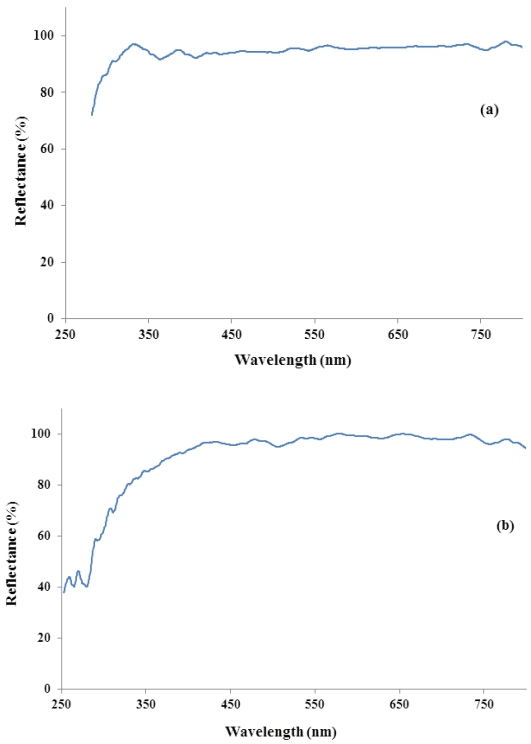

Fig. 10. UV–Vis DRS of the as-synthesized (a) gadolinium carbonate and (b) gadolinium oxide nano-particles.

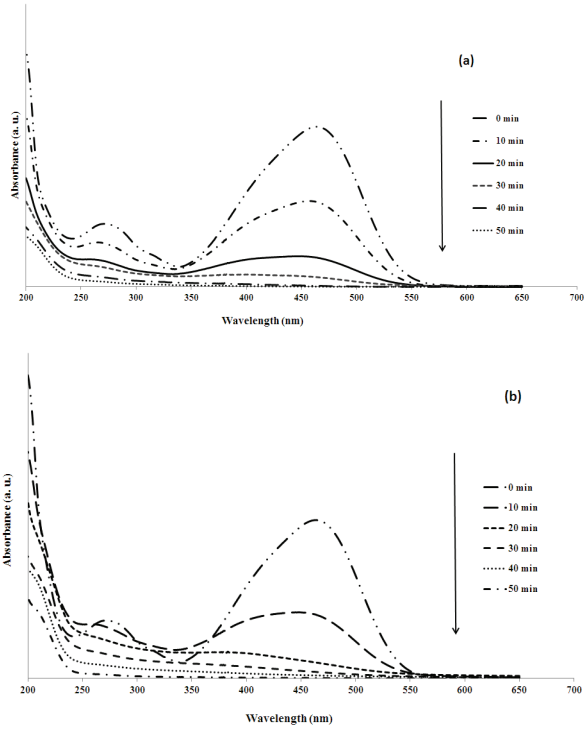

Fig. 12. UV–Vis absorbance spectra of the MO content of an MO solution with the initial concentration of 5 mg/L treated in the presence of 0.1 g/L of (a) gadolinium carbonate, or (b) gadolinium oxide under UV irradiation.

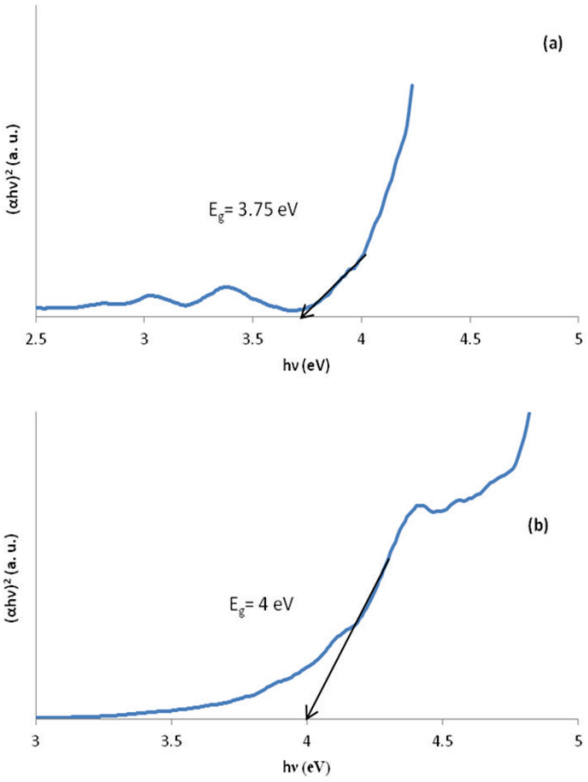

Fig. 11. Tauc's plot obtained for the synthesized (a) gadolinium carbonate and (b) gadolinium oxide nano-particles.

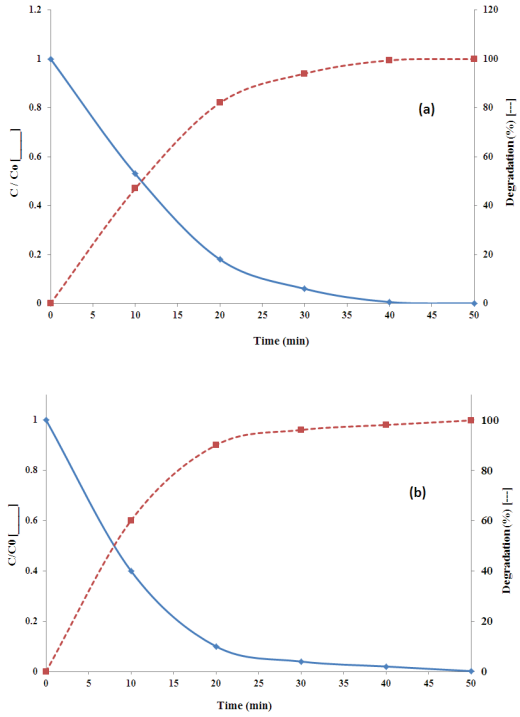

Fig. 13. Photocatalytic degradation of MO solution under UV irradiation using: (a) gadolinium carbonate and (b) gadolinium oxide nano-particles.

from them before starting the reaction as well as 10, 20, 30, 40 and 50 min after the onset of the UV irradiation. These samples were subjected to UV–Vis spectrophotometric analysis to evaluate their MO content (Fig. 12). Also, Fig. 13 illustrates the changes in the MO concentration of the samples as plots of the C/C_0 and degradation efficiency vs. UV–Vis irradiation time. The results clearly show that gadolinium carbonate and oxide nano-particles lead to maximum degradations of 99% and 99.8% after 50 min.

The plots of $-\ln(C/C_0)$ vs. time for the two nano-particles (Fig. 14) are in accordance with pseudo-first-order kinetics behaviors by both nano-structures. The slope of the linear regression provides the reaction rate constants. Table 3 presents the rate constants and maximum conversion values of gadolinium carbonate and oxide, which prove both of these nano-particles as promising photocatalysts for the elimination of MO and other organic pollutants.

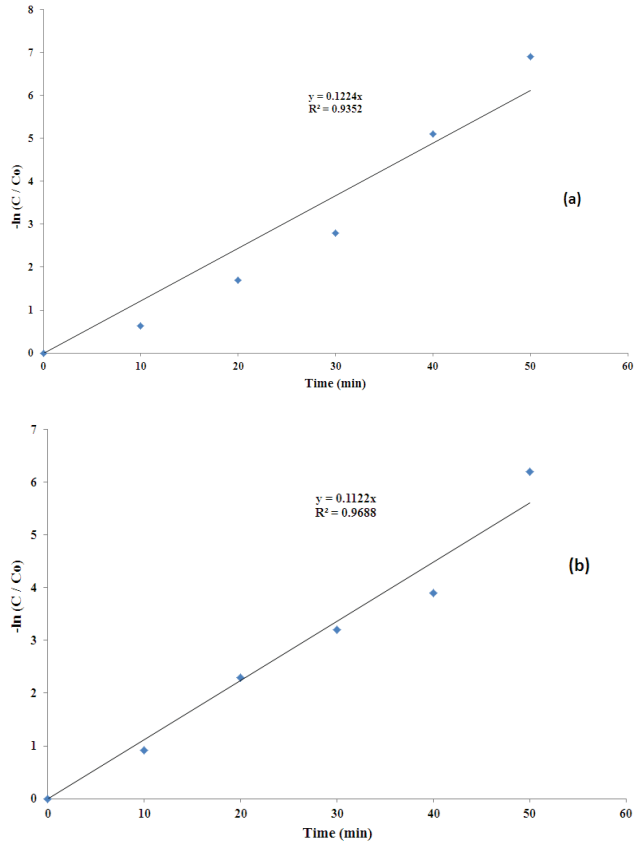

Fig. 14. Pseudo-first-order kinetic behavior during the photodegradation of MO in the presence of (a) gadolinium carbonate and (b) gadolinium oxide nano-particles.

Table 3
Pseudo-first-order reaction rate constant and conversion efficiency of photocatalysts at 50 min

	K (min^{-1})	Conversion (%)
Gadolinium carbonate	0.1224	99.9
Gadolinium oxide	0.1122	99.8

4. Conclusion

Spherical $Gd_2(CO_3)_3$ and Gd_2O_3 nano-particles were synthesized via DPR and solid-state thermal decomposition reaction, respectively. The factors influencing the precipitation procedure for obtaining desired characteristics were optimized through a Taguchi robust design. The results showed that DPR synthesis of $Gd_2(CO_3)_3$ is dependent on certain reaction parameters tuning of which parameters mainly effects the diameter of the product particles. Results of the ANOVA studies showed that Gd^{3+} and carbonate concentrations and temperature of the reactor are significant parameters in determining the dimensions of the $Gd_2(CO_3)_3$ particles, while the flow rate of the gadolinium solution does not. In the meantime, the results of the study demonstrated that Gd_2O_3 nano-particles can be effectively synthesized through the thermal decomposition of $Gd_2(CO_3)_3$ nano-particles formed through DPR as the precursor. The study showed that the thermal decomposition of the precursor leads to the formation of spherical Gd_2O_3 nano-particles. The proposed optimized methods are rather simple and cost effective, and enjoy good potential for scale up and industrial applications.

Acknowledgment

The financial support of this work by Iran National Science Foundation (INSF) and University of Tehran is gratefully acknowledged.

References

[1] E. Hemmer, T. Yamano, H. Kishimoto, N. Venkatachalam, H. Hyodo, K. Soga, Cytotoxic aspects of gadolinium oxide nanostructures for up-conversion and NIR bioimaging, Acta Biomater., 9 (2013) 4734–4743.
[2] J. Kwo, M. Hong, A.R. Kortan, K.T. Queeney, Y.J. Chabal, J.P. Mannaerts, T. Boone, J.J. Krajewski, A.M. Sergent, J.M. Rosamilia, High ε gate dielectrics Gd_2O_3 and Y_2O_3 for silicon, Appl. Phys. Lett., 77 (2000) 130–132.
[3] G.A.M. Hussein, Formation, characterization, and catalytic activity of gadolinium oxide. Infrared spectroscopic studies, J. Phys. Chem., 98 (1994) 9657–9664.
[4] K. Takahashi, S. Tazaki, J. Miyahara, Y. Karasawa, N. Niimura, Imaging performance of imaging plate neutron detectors, Nucl. Instrum. Methods Phys. Res., Sect. A, 377 (1996) 119–122.
[5] G. Gunduz, I. Uslu, Powder characteristics and microstructure of uranium dioxide and uranium dioxide-gadolinium oxide fuel, J. Nucl. Mater., 231 (1996) 113–120.
[6] S. Bhattacharyya, D.C. Agrawal, Preparation of tetragonal ZrO_2-Gd_2O_3 powder, J. Mater. Sci., 30 (1995) 1495–1499.
[7] Z. Chen, Effects of gadolinia and alumina addition on the densification and toughening of silicon carbide, J. Am. Ceram. Soc., 79 (1996) 530–532.
[8] C.M. Wang, X. Pan, M.J. Hoffmann, R.M. Cannon, M. Ruehie, Grain boundary films in rare-earth-glass-based silicon nitride, J. Am. Ceram. Soc., 79 (1996) 788–792.
[9] E.O. Ahlgren, F.W. Poulsen, Thermoelectric power of doped cerium oxide, J. Phys. Chem. Solid., 57 (1996) 589–599.
[10] S.M. Yeh, C.S. Su, UV induced thermoluminescence in rare earth oxide doped phosphors: possible use for UV dosimetry, Radiat. Prot. Dosim., 65 (1996) 359–362.
[11] H.D. Zeman, F.A. Dibianca, G. Lovhoiden, High-resolution X-ray Imaging with a Gd_2O_3(Eu) Transparent Ceramic Scintillator, Proc. SPIE, Vol. 2432, Medical Imaging 1995: Physics of Medical Imaging, 1995, pp. 454–461.
[12] G.Y. Adachi, N. Imanaka, The binary rare earth oxides, Chem. Rev., 98 (1998) 1479–1514.

[13] L. Eyring, Synthesis of Lanthanide and Actinide Compound, Kluwer Academic, Netherlands, 1991, p. 187.
[14] E. Matijevic, W.P. Hsu, Preparation and properties of monodispersed colloidal particles of lanthanide compounds: I. Gadolinium, europium, terbium, samarium, and cerium(III), J. Colloid Interface Sci., 118 (1987) 506–523.
[15] K.S. Mazdiyasni, L.M. Brown, Influence of dynamic calcination on crystallite growth of submicron rare-earth oxides, J. Am. Ceram. Soc., 54 (1971) 479–483.
[16] Z.K. Heiba, L. Arda, Y.S. Hascicek, Structure and microstructure characterization of the mixed sesquioxides $(Gd_{1-x}Yb_x)_2O_3$ and $(Gd_{1-x}Ho_x)_2O_3$ prepared by sol-gel process, J. Appl. Cryst., 38 (2005) 306–310.
[17] R. Wahab, I.H. Hwang, Y.-S. Kim, H.-S. Shin, Photocatalytic activity of zinc oxide micro-flowers synthesized via solution method, Chem. Eng. J., 168 (2011) 359–366.
[18] R. Wahab, M.A. Siddiqui, Q. Saquib, S. Dwivedi, J. Ahmad, J. Musarrat, A.A. Al-Khedhairy, H.-S. Shin, ZnO nano-particles induced oxidative stress and apoptosis in Hep G2 and MCF-7 cancer cells and their antibacterial activity, Colloids Surf., B, 117 (2014) 267–276.
[19] J.C. Colmenares, R. Luque, J.M. Campelo, F. Colmenares, Z. Karpiński, A.A. Romero, Nanostructured photocatalysts and their applications in the photocatalytic transformation of lignocellulosic biomass: an overview, Materials, 2 (2009) 2228–2258.
[20] R. Wahab, S. Dwivedi, F. Khan, Y.K. Mishra, I.H. Hwang, H.-S. Shin, J. Musarrat, A.A. Al-Khedhairy, Statistical analysis of gold nano-particle-induced oxidative stress and apoptosis in myoblast (C2C12) cells, Colloids Surf., B, 123 (2014) 664–672.
[21] R. Wahab, I.H. Hwang, Y.-S. Kim, J. Musarrat, M.A. Siddiqui, H.-K. Seo, S.K. Tripathy, H.-S. Shin, Non-hydrolytic synthesis and photo-catalytic studies of ZnO nano-particles, Chem. Eng. J., 175 (2011) 450–457.
[22] D. Gedamu, I. Paulowicz, S. Kaps, O. Lupan, S. Wille, G. Haidarschin, Y.K. Mishra, R. Adelung, Rapid fabrication technique for interpenetrated ZnO nanotetrapod networks for fast UV sensors, Adv. Mater., 26 (2014) 1541–1550.
[23] Y.K. Mishra, S. Kaps, A. Schuchardt, I. Paulowicz, X. Jin, D. Gedamu, S. Freitag, M. Claus, S. Wille, A. Kovalev, S.N. Gorb, R. Adelung, Fabrication of macroscopically flexible and highly porous 3D semiconductor networks from interpenetrating nanostructures by a simple flame transport approach, Part. Part. Syst. Char., 30 (2013) 775–783.
[24] S. Ghasemi, S. Rahman Setayesh, A. Habibi-Yangjeh, M.R. Hormozi-Nezhad, M.R. Gholami, Assembly of CeO_2-TiO_2 nano-particles prepared in room temperature ionic liquid on graphene nano-sheets for photocatalytic degradation of pollutants, J. Hazard. Mater., 199–200 (2012) 170–178.
[25] M. Barjasteh-Moghaddam, A. Habibi-Yangjeh, Preparation of $Cd(OH)_2$ nanostructures in water using a simple refluxing method and their photocatalytic activity, J. Iran. Chem. Soc., 9 (2012) 163–169.
[26] S.M. Pourmortazavi, S.S. Hajimirsadeghi, M. Rahimi-Nasrabadi, I. Kohsari, Optimization of parameters for the synthesis of silver iodate submicron belts by Taguchi robust design method, Chem. Eng. Comm., 198 (2011) 1182–1188.
[27] S.M. Pourmortazavi, S.S. Hajimirsadeghi, I. Kohsari, R. Fareghi Alamdari, M. Rahimi-Nasrabadi, Determination of the optimal conditions for synthesis of silver oxalate nanorods, Chem. Eng. Technol., 31 (2008) 1532–1535.
[28] M. Rahimi-Nasrabadi, S.M. Pourmortazavi, M. Khalilian-Shalamzari, Facile chemical synthesis and structure characterization of copper molybdate nano-particles, J. Mol. Struct., 1083 (2015) 229–235.
[29] S.M. Pourmortazavi, I. Kohsari, S.S. Hajimirsadeghi, Electrosynthesis and thermal characterization of basic copper carbonate nanoparticles, Cent. Eur. J. Chem., 7 (2009) 74–78.
[30] S.M. Pourmortazavi, M. Rahimi-Nasrabadi, S.S. Hajimirsadeghi, Applying the Taguchi robust design to optimization of the experimental conditions for synthesis of lead chromate nano-rods, J. Dispersion Sci. Technol., 33 (2012) 254–257.
[31] K. Adib, M. Rahimi-Nasrabadi, Z. Rezvani, S.M. Pourmortazavi, F. Ahmadi, H.R. Naderi, M.R. Ganjali, Facile chemical synthesis of cobalt tungstates nanoparticles as high performance supercapacitor, J. Mater. Sci. - Mater. Electron., 27 (2016) 4541–4550.
[32] M. Shamsipur, S.M. Pourmortazavi, S.S. Hajimirsadeghi, M.M. Zahedi, M. Rahimi-Nasrabadi, Facile synthesis of zinc carbonate and zinc oxide nano-particles via direct carbonation and thermal decomposition, Ceram. Int., 39 (2013) 819–827.
[33] S.M. Pourmortazavi, M. Rahimi-Nasrabadi, A.A. Davoudi-Dehaghani, A. Javidan, M.M. Zahedi, S.S. Hajimirsadeghi, Statistical optimization of experimental parameters for synthesis of manganese carbonate and manganese oxide nano-particles, Mater. Res. Bull., 47 (2012) 1045–1050.
[34] S.M. Pourmortazavi, S.S. Hajimirsadeghi, M. Rahimi-Nasrabadi, I. Kohsari, Electrosynthesis and characterization of copper oxalate nano-particles, Synth. React. Inorg. Met.-Org. Chem., 42 (2012) 746–751.
[35] M. Rahimi-Nasrabadi, S.M. Pourmortazavi, Z. Rezvani, K. Adib, M.R. Ganjali, Facile synthesis optimization and structure characterization of zinc tungstate nanoparticles, Mater. Manuf. Processes, 30 (2015) 34–40.
[36] M. Rahimi-Nasrabadi, S.M. Pourmortazavi, M.R. Ganjali, P. Novrouzi, F. Faridbod, M. Sadeghpour Karimi, Preparation of dysprosium carbonate and dysprosium oxide efficient photocatalyst nano-particles through direct carbonation and precursor thermal decomposition, J. Mater. Sci. - Mater. Electron., 28 (2017) 3325–3336.
[37] S.M. Pourmortazavi, M. Taghdiri, V. Makari, M. Rahimi-Nasrabadi, Procedure optimization for green synthesis of silver nanoparticles by aqueous extract of *Eucalyptus oleosa*, Spectrochim. Acta, Part A, 136 (2015) 1249–1254.
[38] S.M. Pourmortazavi, S.S. Hajimirsadeghi, M. Rahimi-Nasrabadi, M.M. Zahedi, Taguchi robust design to optimize synthesis of lead oxalate nano-disks, Mater. Sci. Semicond. Process., 16 (2013) 131–137.
[39] M. Rahimi-Nasrabadi, S.M. Pourmortazavi, M.R. Ganjali, A.R. Banan, F. Ahmadi, Synthesis procedure optimization and characterization of europium (III) tungstate nanoparticles, J. Mol. Struct., 1074 (2014) 85–91.
[40] S.M. Pourmortazavi, M. Rahimi-Nasrabadi, M. Khalilian-Shalamzari, H.R. Ghaeni, S.S. Hajimirsadeghi, Facile chemical synthesis and characterization of Copper Tungstate nanoparticles, J. Inorg. Organomet. Polym., 24 (2014) 333–339.
[41] M. Rahimi-Nasrabadi, S.M. Pourmortazavi, M. Khalilian-Shalamzari, S.S. Hajimirsadeghi, M.M. Zahedi, Optimization of synthesis procedure and structure characterization of manganese tungstate nanoplates, Cent. Eur. J. Chem., 11 (2013) 1393–1401.
[42] S.M. Pourmortazavi, M. Taghdiri, N. Samimi, M. Rahimi-Nasrabadi, Eggshell bioactive membrane assisted synthesis of barium tungstate nanoparticles, Mater. Lett., 121 (2014) 5–7.
[43] M. Rahimi-Nasrabadi, S.M. Pourmortazavi, M.R. Ganjali, S.S. Hajimirsadeghi, M.M. Zahedi, Electrosynthesis and characterization of zinc tungstate nanoparticles, J. Mol. Struct., 1047 (2013) 31–36.
[44] J. Tauc, R. Grigorovici, A. Vancu, Optical properties and electronic structure of amorphous germanium, Phys. Status Solidi B, 15 (1966) 627–637.
[45] K.B. Jaimy, K. Vidya, H.U.N. Saraswathy, N.Y. Hebalkar, K.G.K. Warrier, Dopant-free anatase titanium dioxide as visible-light catalyst: Facile sol-gel microwave approach, J. Environ. Chem. Eng., 3 (2015)1277–1286.
[46] M. Shamsipur, S.M. Pourmortazavi, M. Roushani, S.S. Hajimirsadeghi, Electrochemical preparation and thermal characterization of copper sulfide nanoparticles, Synth. React. Inorg. Met.-Org. Chem., 44 (2014) 951–958.
[47] M. Rahimi-Nasrabadi, S.M. Pourmortazavi, A.A. Davoudi-Dehaghani, S.S. Hajimirsadeghi, M.M. Zahedi, Synthesis and characterization of copper oxalate and copper oxide nanoparticles by statistically optimized controlled precipitation and calcination of precursor, CrystEngComm, 15 (2013) 4077–4086.
[48] M. Salavati-Niasari, J. Javidi, F. Davar, A. AminiFazl, Sonochemical synthesis of $Dy_2(CO_3)_3$ nano-particles and their conversion to Dy_2O_3 and $Dy(OH)_3$: effects of synthesis parameters, J. Alloys Compd., 503 (2010) 500–506.